Synthesis and Characterization of Poly(o-ethoxyaniline)/Nano Silica Composite and Study of its Anticorrosion Performance

Hongli Cheng[1,], Chuanbo Hu[2], Xianglan Wang[1], Ziqiang He[1]*

[1] Department of Chemical and Environmental Engineering, Wuhan Institute of Bioengineering, Wuhan 430415, China
[2] School of Metallurgy, Northeastern University, Shenyang 110819, China
[*]E-mail: chl20111027@126.com

The poly(o-ethoxyaniline)/nano silica (POEA/SiO$_2$) composite material was synthesized by in-situ polymerization method. The structure, composition and morphology were characterized by Fourier transform infrared spectroscopy (FT-IR), UV-visible adsorption spectroscopy (UV-vis), X-ray diffraction patterns (XRD) and field emission scanning electron microscopy (SEM). The thermal stability was studied by Thermogravimetric analysis (TGA). The electrochemical behaviors were performed by cyclic voltammetry (CV) technique. Epoxy coatings containing SiO$_2$ nanoparticles, POEA and POEA/SiO$_2$ powders were prepared on the surface of the treated carbon steel. The surface morphology of the coatings was observed by FESEM, the electrochemical corrosion behavior was studied by Tafel polarization curve and electrochemical impedance spectroscopy (EIS) in 3.5% NaCl solution. The results show that the POEA/SiO$_2$ containing coating exhibit a lower corrosion rate of 0.02 mm/year and the corrosion protection efficiency is as high as 98.9%. The EIS measurement was also demonstrate that the addition of POEA/SiO$_2$ could improve the anticorrosion performance of epoxy coating significantly than that of POEA and SiO$_2$ nanoparticles.

1. INTRODUCTION

Corrosion usually refers to a chemical or electrochemical action that occurs between the metallic material and the environmental medium, resulting in the destruction or degradation of the material. Corrosion is an irreversible process since the use of metallic materials. Metal corrosion to human's production and life causes a serious harm and huge waste of resources. In order to solve the problem of corrosion of metal materials and equipment, the development of high-performance,

pollution-free, economical anticorrosion coatings has become a new trend in the field of anticorrosion coatings [1,2]. The presence of polyaniline (PANI) anticorrosive coatings have brought new opportunities to this problem.

Due to the unique anti-scratch, pitting resistance, low cost, use of various metal anticorrosion and advantages of no impact to the environment [3,4], PANI can be used in marine, aviation and other special conditions. PANI is a new type of metal corrosion protection material with huge commercial prospects. However, the high rigidity of the PANI molecular chain and the strong interaction between chains result in poor processing, solubility and poor mechanical properties [5], which greatly restrict its application and development. It has been found that PANI derivatives with weak molecular chains can be obtained by introducing appropriate electron-donating substituents on the PANI ring to improve its solubility in organic solvent, thermal stability and dispersity in the resin coating [6,7]. It was also possible to obtain a PANI derivative coating excellent in compactness and corrosion resistance [8,9]. In fact, the solubility of some substituted PANIs such as poly(o-ethoxyaniline) (POEA) has increased in some solvents, and even can improve the solubility in the aqueous medium in some special cases [10]. Chaudhari et al. [11] used POEA coating to protect the copper and had obtained satisfied with the results. SiO_2 nanoparticles can improve the anti-aging, strength and chemical resistance of other materials. The SiO_2 nanoparticles fully and evenly dispersed into the resin material can comprehensively improve the performance of resin-based materials, such as the improvment of its strength, elongation and wear resistance, and it can also improve the surface finish and anti-aging properties of the material [12,13]. In this paper, a new metal anticorrosion material POEA/SiO_2 composite was synthesized by in-situ polymerization. Epoxy coating including POEA/SiO_2 composite was prepared on the surface of carbon steel, and the corrosion protection efficiency of epoxy/POEA/SiO_2 coating on steel substrate was studied by Tafel polarization curve and electrochemical impedance spectroscopy (EIS) in 3.5% NaCl solution as corrosive environment.

2. EXPERIMENTAL

2.1 Materials

O-ethoxyaniline (OEA), hydrochloric acid (HCl), ammonium persulfate (APS), acetone, sodium chloride (NaCl), ethanol, butyl alcohol, N-Methyl-2-Pyrrolidone (NMP), dibutyl phthalate (DBP) and ethyl acetate, and the above reagents were purchased from different resources and used without further purification. Epoxy resin (EP) and polyamide (651) were purchased from Yichun Yunda Chemical Co., Ltd. Silica (SiO_2) with average particle size of 20 nm was supplied by Shanghai Maikun Chemical Co., Ltd.

2.2 Synthesis of POEA/SiO$_2$ composite

The POEA/SiO_2 composite was synthesized by in-situ polymerization with HCl as dopant, OEA monomer was distilled to colorless before use. The experimental procedure was as follows: 13.05

mL of OEA monomer was added to 100 mL 1.0 M of HCl soulution to from a clarifying solution under stirring. Then, a certain amount of SiO_2 powder was ultrasonically dispersed in deionized water and added the OEA-HCl solution stirred for 30 min at room temperature to obtain a uniformly emulsion. After that, the mixed emulsion was added to a three-necked flask and continued stirred for 30 min, and then 100 mL of 1.0 M APS solution was added dropwise to the mixture solution within 2 h under vigorous stirring. The resulting mixture was allowed to react below 5 °C for 10 h. The precipitate was filtered and washed with ethanol and deionized water. Finally, the filter cake was dried in oven at 60 °C for 24 h and then fine grinded by agate mortar before used as fillers. Pure POEA was also synthesized by the same method without the use of SiO_2.

2.3 Characterization

The FT-IR spectra of samples were recorded using a Perkin Elmer FTIR RXI spectrometer in the region of 4000–500 cm^{-1} by the KBr pellets method. The UV–vis spectra of samples were performed using Shimadu UV2550 spectrophotometer in the range 250–850 nm. The XRD patterns of samples were taken with an UltimaIV X-ray diffractometer using Cu *Kα* radiation in the 2θ range of 10–90∘. The SEM images of the samples were performed on SU8010 field emission scanning electron microscopy. The TGA curves of samples were performed on HCT-1 analyzer in air from 25 to 800 °C at the heating rate of 10 °C/min. The CV measurements were performed on Princeton 2273 electrochemical workstation, the electrolyte was 1.0 M HCl solution. A typical three-electrode cell was used with a platinum plate as the counter electrode and a saturated calomel electrode (SCE) as the reference electrode, a piece of carbon paper loaded with POEA or POEA/SiO_2 was used as the working electrode.

2.4 Preparation of the coatings

The carbon steel samples with the size of 2cm × 2cm were polished into a mirror with metallographic sandpaper of 100, 360, 600, 1000 and 1200 mesh respectively in the MP-1B polishing machine. The samples were immersed in acetone and ethanol solution ultrasonic 30 min to remove oily be soiled, and then air-dried at room temperature before coated. For preparation of the coatings, 2.5 g of epoxy resin was weighed into a beaker, and a mixed solvent consisting of 0.75 mL of dibutyl phthalate and 0.25 mL of NMP and 0.75 g of curing agent were successively added, mechanically stirred uniformly, and then 0.24 mL of plasticizer DBP and 0.28 mL of ethyl acetate were added with ultrasonic dispersion 30min to ensure uniform dispersion. The coating materials were uniformly applied to the treated carbon steel substrates and cured at 60 °C in oven for 24 h to obtain an epoxy resin coating (epoxy). The epoxy/SiO_2 coating, epoxy/POEA coating and epoxy/POEA/SiO_2 coating were also obtained by using SiO_2 nanoparticles, POEA and POEA/SiO_2 as the materials based on epoxy resin. Figure 1 shows the schematic preparation of the HCl doped epoxy/POEA/SiO_2 composite coating onto the surface of carbon steel.
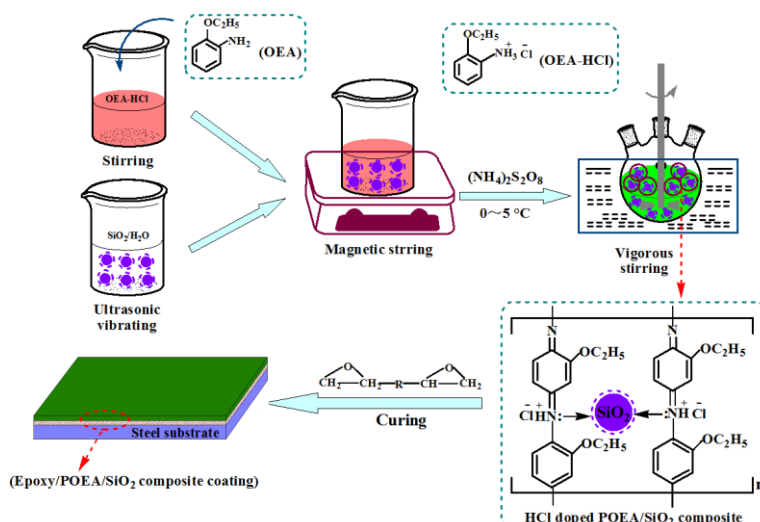
Figure 1. The schematic preparation of HCl doped epoxy/POEA/SiO$_2$ composite coating onto the carbon steel substrate.

2.5 Evaluation of the coatings

The anticorrosion performances of the coatings on the surfaces of carbon steel were tested. The Tafel polarization curves and electrochemical impedance spectroscopy of the coated samples were tested after immersed in 3.5% NaCl solution for a period of time using the Princeton 2273 electrochemical workstation. A three-electrode system was used with a SCE was used as the reference electrode, the platinum electrode (Pt) was the counter electrode, and the coated carbon steel sample was the working electrode. The Tafel Polarization Curve test has a scanning voltage range of –0.25~0.25 V at open circuit potential and scan rate of 1 mV/s. The EIS test was performed at a frequency region from 100 kHz to 10 mHz with an AC amplitude of 10 mV.

3. RESULTS AND DISCUSSION

3.1 Structure and morphology

Figure 2 shows the FTIR spectra of SiO$_2$, POEA and POEA/SiO$_2$. It can be seen from Fig. 2(a) that the FTIR spectrum of SiO$_2$ is consistent with the literature [14]: The broad peak at 3435 cm^{-1} is the structure of water–OH antisymmetric stretching vibration. The peak near 1632 cm^{-1} is the H–O–H bending vibration peak of water. The strong and wide absorption at 1096 cm^{-1} is the Si–O–Si antisymmetric stretching vibration. The peak at 963cm^{-1} is the peak of Si–OH bending vibration. The peaks at 806 cm^{-1} and 474cm^{-1} are the Si–O symmetric stretching and bending vibrations. Fig. 2(b) shows the FTIR spectra of POEA and POEA/SiO$_2$ composite. As shown in Fig. 2(b), the FTIR spectrum of POEA is consistent with those of literature [15-17]. The main characteristic absorption peaks are as follows: the peak of 2983 cm^{-1} is caused by the expansion vibration of =C–H on the benzene ring. The peaks of 1499 cm^{-1} and 1572 cm^{-1} are respectively caused by the stretching vibration

of N–B–N and the stretching force of N=Q=N. The peak of 1294 cm^{-1} is the absorption peak of C–N stretching vibration. The peak of 1120 cm^{-1} is the characteristic absorption peak of the ether bond, which is caused by the asymmetric stretching vibration of the C–O–C. The peak of 818 cm^{-1} indicates that 1,2,4-positions have been substituted in the benzene ring. For POEA/SiO$_2$ composite, the main characteristic peaks of POEA exist in the composite and there is slight shift of the POEA peaks. It is shown that the polymer covered on the surface of the nanoparticles, resulting in the certain interaction existed between POEA and SiO$_2$ [18]. The characteristic peak of SiO$_2$ has turned to weaken in composite or overlapped with the peaks of POEA, these results implies that SiO$_2$ have been effectively covered by POEA.
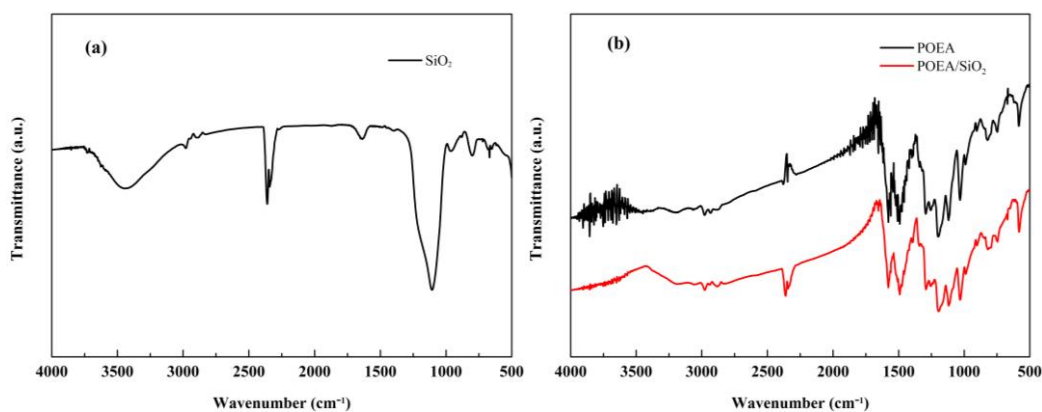
Figure 2. FT-IR spectra of (a) SiO$_2$ nanoparticles and (b) POEA and POEA/SiO$_2$ composite.

Figure 3 shows the UV-Vis spectra of POEA and POEA/SiO$_2$. As shown in Fig. 3, the characteristic peaks of these two polymer materials are basically the same. The main characteristic peaks are as follows: there is a strong absorption peak at the wavelength of 303 nm, which belongs to π–π* electron transition of benzene ring structure in POEA. The broad and weak absorption peak at the wavelength of 605 nm, which belongs to the n–π* transition of the quinoid ring in POEA [19,20]. As present in Fig. 3(b), the characteristic peaks of POEA/SiO$_2$ were red shifted to 312 and 618 nm, respectively, and the absorption intensity has increased, which was due to the similar hydrogen bond interaction between SiO$_2$ and POEA that affected the regularity and conjugation of POEA chains.
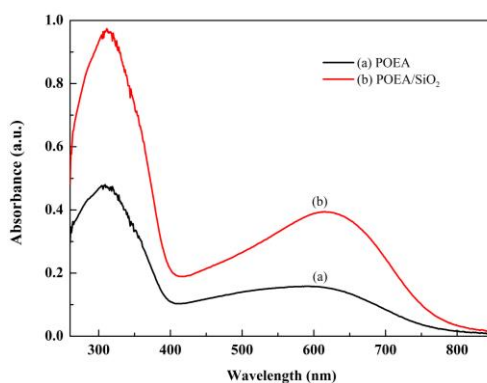
Figure 3. UV-vis spectra of (a) POEA and (b) POEA/SiO$_2$ composite.

Figure 4 shows the XRD patterns of SiO_2, POEA and $POEA/SiO_2$. It can be seen from Fig. 4(a) that there is no obvious diffraction peak of SiO_2, but a large peak package appears at $2\theta=23°$, the observed 2θ value is consistent with the standard JCPDS values (JCPDS No. 29-0085). As shown in Fig. 4(c), the XRD patterns of $POEA/SiO_2$ has the diffraction characteristics of POEA and SiO_2, except that the diffraction peak intensity is enhanced with respect to POEA and SiO_2, indicating that the crystal behavior after composite modification is enhanced. This is due to the fact that the POEA molecules in the crystalline form are covered on the surface of the SiO_2 nanoparticles, increasing the mass-volume percentage of the nanoparticles to produce the diffraction conditions [21,22], thus enhancing the characteristic diffraction peaks of the $POEA/SiO_2$. Furthermore, the two diffraction peaks appear at $2\theta=23.5°$ and $2\theta=24.8°$ which representing the periodic parallelism and verticality of the POEA chain respectively, and it illustrates the whole order of the POEA materials.
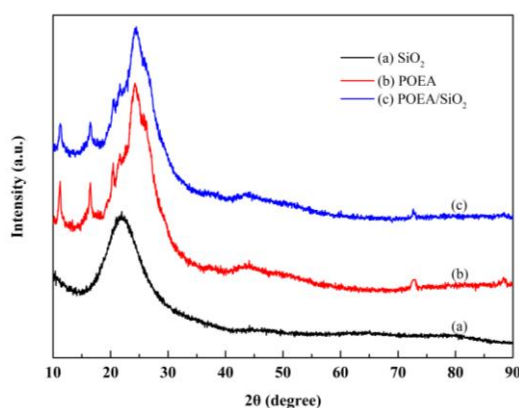
Figure 4. XRD patterns of (a) SiO_2 nanoparticles, (b) POEA and (c) $POEA/SiO_2$ composite.
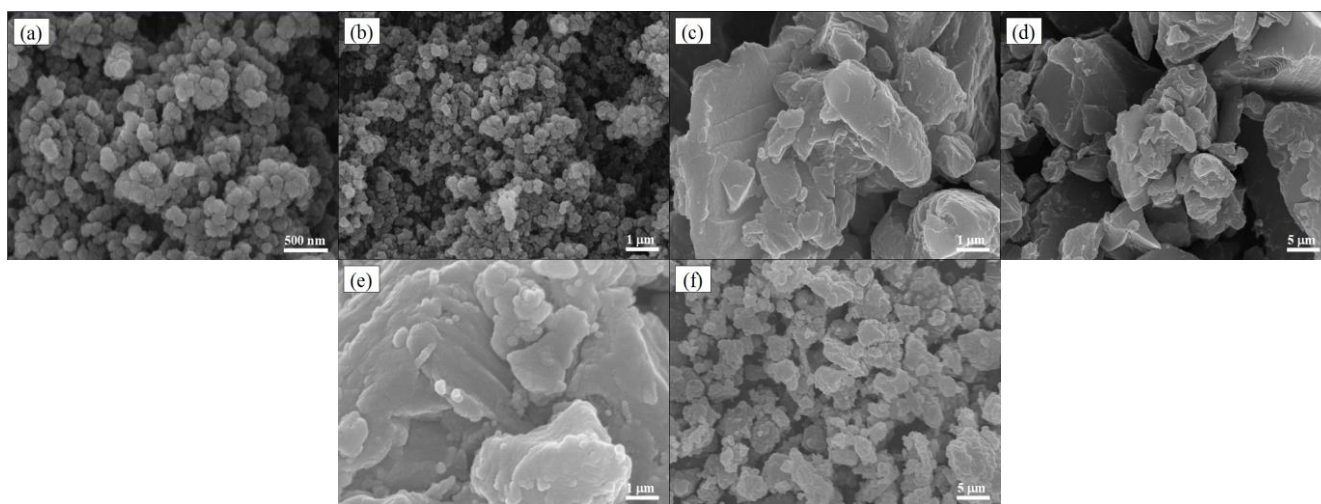
Figure 5. SEM images of (a-b) SiO_2 nanoparticles, (c-d) POEA and (e-f) $POEA/SiO_2$ composite.

Figure 5 shows the SEM images of SiO_2, POEA and $POEA/SiO_2$. Fig. 5 (a-b) show that the uniform size of the SiO_2 nanoparticles are clustered together and the distribution is more uniform and dense. Fig. 5 (c-d) show that the POEA is composed of various pieces of different sizes and connected

together, having certain porosity and poor density. Fig. 5(e-f) show that POEA/SiO$_2$ is composed of particles that dispersed together of relatively uniform size. The results indicating that when SiO$_2$ nanoparticles are dispersed in OEA-HCl solution, the OEA monomer is polymerized on the surface of the inorganic nanoparticles with smaller particle size under the action of oxidant, so that the SiO$_2$ nanoparticles are covered inside the POEA molecule to improve the pore defects of the polymer.

Figure 6 shows the TGA curves of POEA and POEA/SiO$_2$. It can be seen that the thermal loss curves of POEA and POEA/SiO$_2$ are similar, and the weight loss process is divided into two stages [23,24]. For POEA, the first stage recorded at 25~117 °C, the weight loss at this stage is mainly caused by the physical adsorption of water molecules of POEA. The second stage starts at 220 °C, this stage of the sample weight loss is obvious for the POEA loss of dopants and the degradation of POEA chains. From Fig. 6(b), it can be seen that the TGA curves of POEA/SiO$_2$ composites are similar to that of POEA, but the degradation rate of POEA/SiO$_2$ is lower at the corresponding weight loss stage. When the temperature rose to 800 °C, the weightlessness percentages of POEA and POEA/SiO$_2$ were 57.1% and 47.3% respectively, which indicates that the thermal stability of POEA/SiO$_2$ was better than that of POEA. The better thermal stability may be due to the good contact and intermolecular force between POEA and SiO$_2$ nanoparticles, thus it improves the steric hindrance effect of POEA chains and inhibits the molecular chain's hot motion to some extent [25].
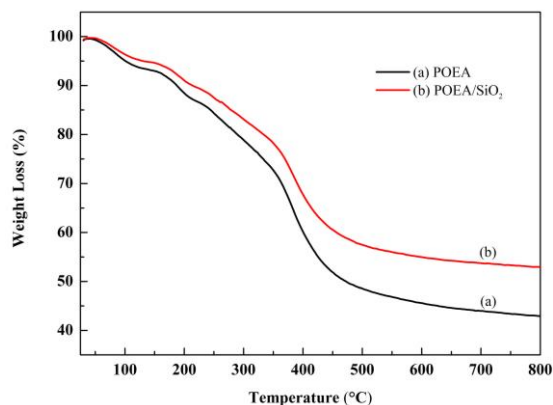
Figure 6. TGA curves of (a) POEA and (b) POEA/SiO$_2$ composite.

3.2 Electrochemical behavior

The electrochemical activity and stability of POEA and POEA/SiO$_2$ were tested by CV technique at a scan rate of 20 mV/s between –0.2 and 1.0 V. Fig. 7(a) is a CV curves of POEA and POEA/SiO$_2$ in 1.0 M HCl solution. It can be seen that both polymer materials exhibited the electrochemical characteristic of PANI, two pairs of redox peaks in the CV curves of POEA and POEA/SiO$_2$ films were attributed to the leucoemeraldine/emeraldine and emeraldine/pernigraniline transitions of POEA, which indicating the pseudocapacitance behavior of the conducting polymer [26]. It was noted that both POEA and POEA/SiO$_2$ have reversible electrochemical activity. The potential difference ΔEp of the oxidation potential and the reduction potential is used to estimate the reversibility of redox reaction [27]. The closer the ΔEp value is to zero, the better the electrochemical

reversibility [28]. Differences ΔEp of POEA were 0.09 and 0.21 V, and that of POEA/SiO$_2$ were 0.08 and 0.18 V, respectively. The results indicate that the electrochemical reversibility of POEA/SiO$_2$ is better than that of POEA, and the addition of SiO$_2$ nanoparticles improves the electrochemical activity of POEA. In addition, the redox peak current of POEA/SiO$_2$ is obviously higher than that of POEA, which indicates that the presence of SiO$_2$ nanoparticles are favorable for the redox reaction of POEA chains, and the electrochemical activity of POEA/SiO$_2$ is higher than that of POEA. Fig. 7(b) is a CV curves for continuously scanning 10 cycles of POEA and POEA/SiO$_2$ at a rate of 20 mV/s. It can be seen that the CV curves of POEA and POEA/SiO$_2$ changes smaller after 10 cycles continuous scanning. The results indicate that POEA and POEA/SiO$_2$ have excellent electrochemical stability.
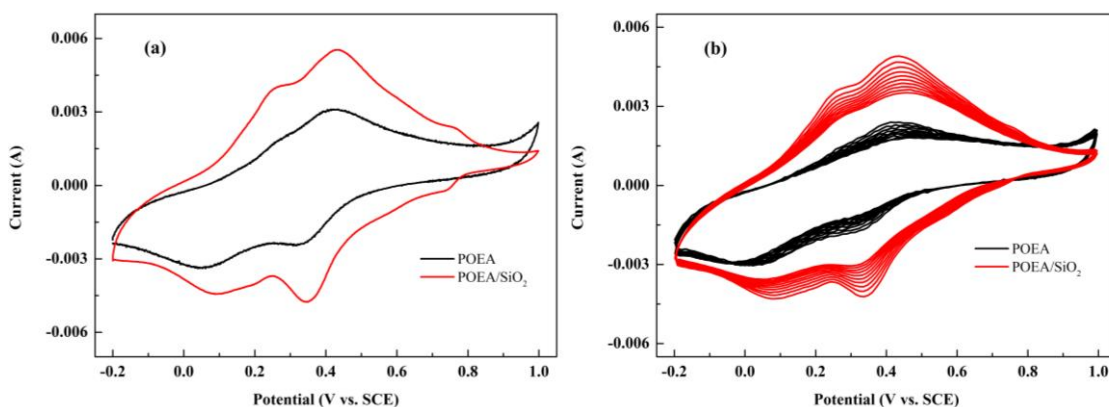
Figure 7. CV curves of POEA and POEA/SiO$_2$ composite films immersed in 1.0 M HCl solution: (a) a separate ring and (b) consecutively scanning 10 cycles at 20 mV/s scan rate.

3.3 Surface characterization
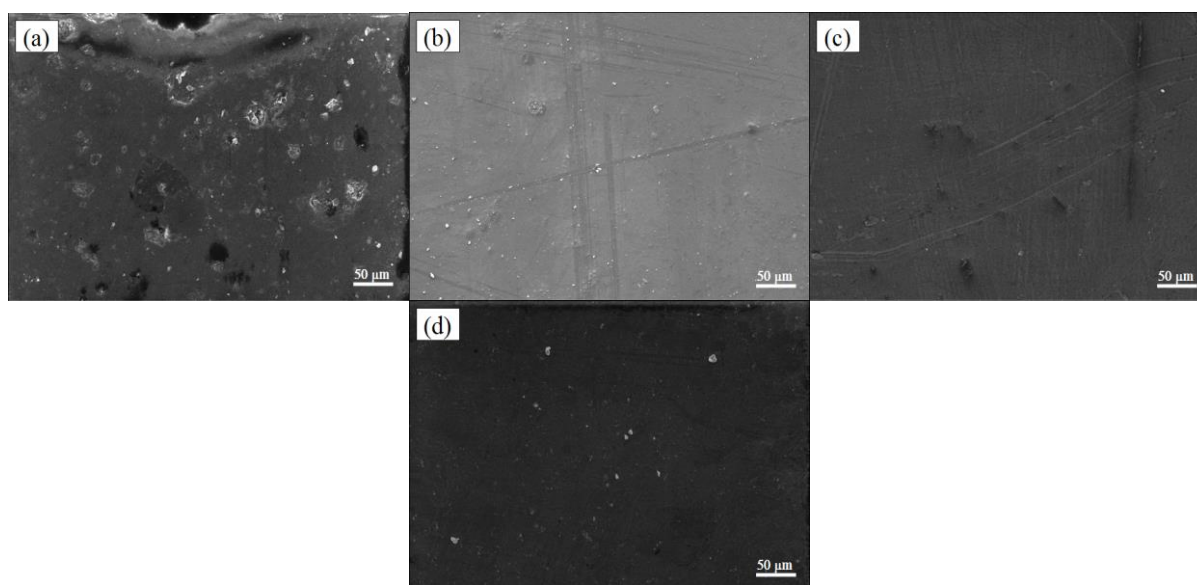
Figure 8. SEM images the surface of (a) epoxy, (b) epoxy/SiO$_2$, (c) epoxy/POEA and (d) epoxy/POEA/SiO$_2$ coatings.

Figure 8 shows the surface topography of epoxy, epoxy/SiO$_2$, epoxy/POEA and epoxy/POEA/SiO$_2$ coatings. It can be seen from Fig. 8(a) that there are some cracks and pores in the epoxy coating due to the evaporation of solvent, which can easily cause the defects of the coating and the poor density. As can be seen from Fig. 8(b-d), the coating defects have decreased when the fillers were added into the epoxy resin. Fig. 8(b) shows that the addition of SiO$_2$ nanoparticles improved the compactness of the coating but there are micropores still. Fig. 8(c-d) shows that the surfaces of the epoxy/POEA and epoxy/POEA/SiO$_2$ coatings is free of cracks, uniform and compact, and the surface of epoxy/POEA/SiO$_2$ coating is smoother. This is due to the excellent compatibility between the POEA/SiO$_2$ and epoxy resin. When POEA and POEA/SiO$_2$ are dispersed in the epoxy resin, the fillers can block the pores to form a uniform and compact composite coating.

3.4 Corrosion protection evaluation

Figure 9 shows the Tafel polarization curves of bare steel and steel samples coated with epoxy, epoxy/SiO$_2$, epoxy/POEA and epoxy/POEA/SiO$_2$ coatings immersed in 3.5% NaCl solution for a period of time. E_{corr} is the corrosion potential and I_{corr} is the corrosion current density. The corrosion parameters of coating samples were obtained by Tafel extrapolation method [29] as shown in Table 1. The equation of corrosion rate C_R can be calculated as follows [30]:

$$C_R = 3270 \times \frac{M(g) \cdot I_{corr}(A/cm^2)}{n \cdot \rho(g/cm^3)}$$

In the formula, M is the weight molecular of carbon steel, I_{corr} is the corrosion current density, n is the number of electrons lost in the oxidation reduction process, ρ is the density of carbon steel. Correspondingly, the corrosion protection efficiency of the coating can be obtained by the following equation [31]:

$$PE(\%) = \frac{I_{corr} - I_{corr(c)}}{I_{corr}} \times 100 \%$$

where I_{corr} is the corrosion current density of bare steel, $I_{corr(c)}$ is the corrosion current density of coated steel. Usually, the fitted Tafel polarization curves have higher E_{corr} but lower I_{corr} and C_R, indicating that the coating possess better anticorrosion performance [32,33]. As can be seen from the data in Table 1, the E_{corr} of the carbon steel coated with epoxy, epoxy/SiO$_2$, epxoy/POEA, epoxy/POEA/SiO$_2$ coating were gradually increased compared with the bare steel, the I_{corr} and C_R were gradually decreases. The corrosion parameters of the coated samples containing the fillers composition are better than those of the epoxy coating. The corrosion protection ability follows the order of epoxy<epoxy/SiO$_2$<epoxy/POEA<epoxy/POEA/SiO$_2$ coatings. For bare steel, because there is no anything protective coating, the electrolyte solution would attack the steel substrate when the substrate was exposed in corrosive media. Due to the interaction between POEA and SiO$_2$ nanoparticles, when the corrosive medium begins to contact with the coating film, the micro/nanostructures on the surface of the coating have a certain barrier effects to the active Cl^{-1} and water-eroded media in the corrosive medium, and thus increased the barrier effect of the composite coating to the corrosive medium [34], and make the corrosion protection of the POEA/SiO$_2$ containing coating is the best.
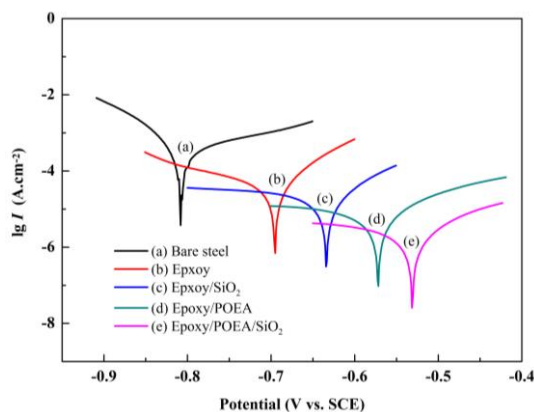
Figure 9. Tafel plots of (a) bare steel, (b) epoxy, (c) epoxy/SiO$_2$, (d) epoxy/POEA and (e) epoxy/POEA/SiO$_2$ coatings immersed in 3.5% NaCl solution for a period of time.

Table 1. Fitting corrosion parameters for bare and coated steel samples immersed in 3.5% NaCl solution by Tafel polarization measurement.

Samples	E_{corr} (mV)	I_{corr} (A/cm^2)	C_R (mm/a)	PE (%)
Bare steel	−0.802	$1.69×10^{-4}$	1.98	/
Epoxy	−0.698	$5.01×10^{-5}$	0.59	70.3
Epoxy/SiO$_2$	−0.638	$2.23×10^{-5}$	0.26	86.8
Epoxy/POEA	−0.576	$8.13×10^{-6}$	0.09	95.2
Epoxy/POEA/SiO$_2$	−0.532	$1.78×10^{-6}$	0.02	98.9

The EIS was also performed to evaluate the anticorrosion performance of the carbon steel samples coated with epoxy, epoxy/SiO$_2$, epoxy/POEA and epoxy/POEA/SiO$_2$ coatings. Figure 10 shows the EIS plots of bare and coated steel samples immersed in 3.5% NaCl solution for a period of time. It is possible to use the diameter of the formed semicircle in EIS plots as an indicator of the corrosion rate. Generally, the impedance Z depends on the charge transfer resistance R_{ct}, the solution resistance R_s, the double layer capacitance C_{dl} and the frequency of the AC signal ω. The impedance can be describes as follow [35]:

$$Z = Z' + jZ'' = R_s + \frac{R_{ct}}{1+(R_{ct}C_{dl}\omega)^2} + j\frac{R_{ct}^2 C_{dl}\omega}{1+(R_{ct}C_{dl}\omega)^2}$$

In the EIS plots, the high frequency intercept of the real part of impedance is equivalent to R_s, the low frequency intercept is equivalent to the sum of R_s and R_{ct}. Therefore, the R_{ct} was estimated as the difference between the high and low frequency intercepts. The larger the diameter of the semicircle indicates the smaller the corrosion rate [36]. It is observed from Fig. 10 that the EIS plots of all coatings display the similar characteristics. There is a depressed semicircle in all the low frequency and no diffusion impedance in the high frequency. From Fig. 10(a), the EIS plots depict that the bare steel possess the lowest arc resistance and impedance values, indicating that the four coatings can be used to protection the steel anticorrosion. Due to the role of epoxy resin, epoxy coating has a certain anticorrosion performance, but its corrosion resistance is poor compared with other coatings because

the existence of the pores after solvent evaporation. Epoxy/POEA coating contains POEA filler, which can improve the corrosion resistance of the coating. The carbon steel coated with epoxy/POEA/SiO$_2$ composite has the highest diameter, it indicate that the corrosion protection is the best. This is mainly attributed to the addition of SiO$_2$ nanoparticles can enhance the uniformity and density of the coating surface. So that it act as a barrier that increase the tortuosity of the diffusion pathway of oxygen, water and chloride ions.
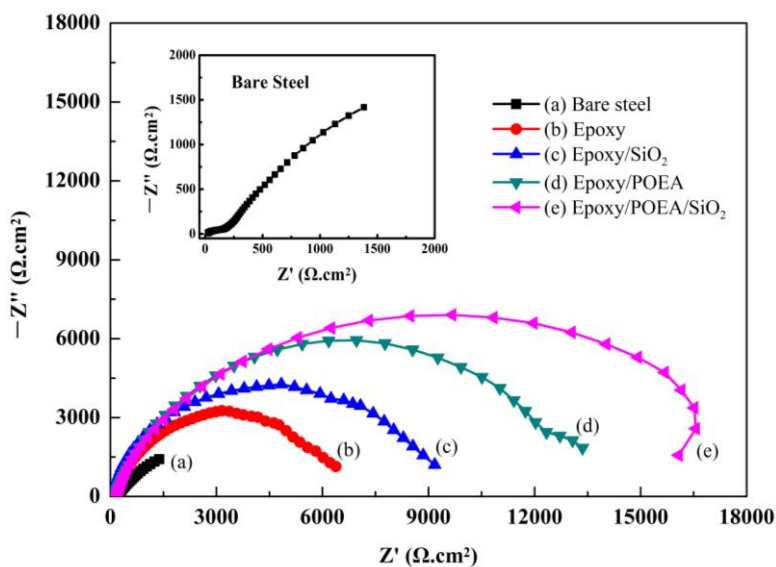
Figure 10. EIS plots of (a) bare steel, (b) epoxy, (c) epoxy/SiO$_2$, (d) epoxy/POEA and (e) epoxy/POEA/SiO$_2$ coatings immersed in 3.5% NaCl solution for a period of time.

4. CONCLUSIONS

In this paper, POEA/SiO$_2$ composite has been successfully synthesized by in-situ polymerization method with hydrochloric acid as dopant. The analysis of structure and morphology shows that there is a certain interaction between POEA and SiO$_2$ nanoparticles. The electrochemical behavior analysis indicates that POEA/SiO$_2$ composite is reversible and stable. The corrosion studies of all coated steel in 3.5% NaCl solution by Tafel polarization curves and electrochemical impedance spectroscopy have shown that epoxy/POEA/SiO$_2$ coating possess the higher anticorrosion ability than those of epoxy/POEA, epoxy/SiO$_2$ and epoxy coatings. The corrosion protection efficiency of epoxy/POEA/SiO$_2$ coating to steel substrate can up to 98.9%. So it can concluded that POEA/SiO$_2$ composite proves to be an effective inhibitor for metal corrosion and it has potential industrial applications in the near future.

References

1. L. Ma, F.F. Chen, Z.T. Li, M.Y. Gan, J.Yan, S.J. Wei, Y.Q. Bai and J. Zeng, *Compos. Part B: Eng.,* 58 (2014) 54.
2. P. He, J.X. Wang, F.Y. Lu, Q. Ma and Z. Wang, *Prog. Org. Coat.,* 110 (2017) 1.
3. A.A. Hermas, M.A. Salama and S.S. Al-Juaid, *Prog. Org. Coat.,* 76 (2013) 1810.
4. A.H. Navarchian, M. Joulazadeh and F. Karimi, *Prog. Org. Coat.,* 77(2014) 347.
5. J.L. Gu, L. Ma, M.Y. Gan, F. Zhang, W.L. Li and C.Q. Huang, *Thermochim. Acta*, 549 (2012) 13.
6. E. Hür, G. Bereket and Y. Şahin, *Curr. Appl. Phys.,* 7 (2007) 597.
7. P.A. Basnayaka, M.K. Ram, E.K. Stefanakos and A. Kumar, *Electrochim. Acta*, 92 (2013) 376.
8. A. Benchikh, R. Aitout, L. Makhloufi, L. Benhaddad and B. Saidani, *Desalination*, 249 (2009) 466.
9. S. Chaudhari, S.R. Sainkar and P.P. Patil, *J. Phys. D: Appl. Phys.,* 40 (2007) 520.
10. J.S. Choi, J.H. Sung, H.J. Choi and M.S. Jhon, *Synth. Met.,* 153 (2005) 129.
11. S. Chaudhari and P.P. Patil, *Electrochim. Acta*, 53 (2007) 927.
12. J.J. Yuan, S.X. Zhou, G.X. Gu and L.M. Wu, *J. Mater. SCI.,* 40 (2005) 3927.
13. S.R. Lu, J.H. Yu, H.L. Zhang and X.Y. Wang, *J. Mater. Sci.,* 40 (2005): 2815.
14. D.Z. Yin, Q.Y. Zhang, H.P. Zhang and C.J. Yin, *J. Polym. Res.,* 17 (2010) 689.
15. P. Cossari, V. Bavastrello and C. Nicolini, *Synth. Met.,* 176 (2013) 1.
16. T. Zhou, S. Tan, Y.L. Guo, L. Ma, M.Y. Gan, H.H. Wang, X.W. Sun and H.N. Wang, *J. Alloys. Compd.,* 652 (2015) 358.
17. A.S. Silva, J.C. Soares, A.C. Mafud, S.M. Souza, E.G.R. Fernandes, Y.P. Mascarenhas and E.A. Sanches, *J. Mol. Struct.,* 1071 (2014) 1.
18. Y.D. Liu, W.L. Zhang and H.J. Choi, *Colloid Polym. Sci.,* 290 (2012) 855.
19. V. Talwar, O. Singh and R.C. Singh, *Sens. Actuators B: Chem.,* 191 (2014) 276.
20. J.J. Li, X.F. Tang, H. Li, Y.G. Yan and Q.J. Zhang, *Synth. Met.,* 160 (2010) 1153.
21. S.G. Pawar , S.L. Patil , M.A. Chougule , A.T. Mane , D.M. Jundale and V.B. Pati, *Int. J. Polym. Mater.,* 59 (2010) 777.
22. Z.A. Hu, Y.L. Xie, Y.X. Wang, L.P. Mo, Y.Y. Yang and Z.Y. Zhang, *Mater. Chem. Phys.,* 114 (2009) 990.
23. B.H. Lee, H.J. Kim and H.S. Yang, *Curr. Appl. Phys.,* 12 (2012) 75.
24. W.F. Alves, E.C. Venancioc, F.L. Leite, D.H. F. Kanda, L.F. Malmonge, J.A. Malmonge and L.H.C. Mattoso, *Thermochim. Acta*, 502 (2010) 43.
25. J. Zhang, D. Shu, T.R Zhang, H.Y. Chen, H.M. Zhao, Y.S. Wang, Z.J. Sun, S.Q. Tang, X.M. Fang and X.F. Cao, *J. Alloys. Compd.,* 532 (2012) 1.
26. H.P. Cong, X.C. Ren, P. Wang and S.H. Yu, *Energy Environ. Sci.,* 2013 (6) 1185.
27. C.Y. Wang, V. Mottaghitalab, C.O. Too, G.M. Spinks and G.G. Wallace, *J. Power Sources*, 163 (2007) 1105.
28. Y.V. Stulov, V.G. Kremenetsky and S.A. Kuznetsov, *Int. J. Electrochem. Sci.,* 8 (2013) 7327.
29. H. Bhandari, S. Sathiyanaranayan, V. Choudhary and S.K. Dhawan, *J. Appl. Polym. Sci.,* 111 (2009) 2318.
30. C.H. Chang, T.C. Huang, C.W. Peng, T.C. Yeh, H.I. Lu, W.I. Hung, C.J. Weng, T.I. Yang and J.M, Yeh, *Carbon*, 50 (2012) 5044.
31. V. Karpakam, K. Kamaraj, S. Sathiyanarayanan, G. Venkatachari and S. Ramu, *Electrochim. Acta*, 56 (2011) 2165.
32. Y.Q. Qing, C.N. Yang, Z.Y. Yu, Z.F. Zhang, Q.L. Hu and C.S. Liu, *J. Electrochem. Soc.,* 163 (2016) D385.
33. J.B. Jiang, Y. Wang, Q.D. Zhong, Q.Y. Zhou and L. Zhang, *Surf. Coat. Technol.,* 206 (2011) 473.
34. E. Akbarinezhad, M. Ebrahimi, F. Sharif, M.M. Attar and H.R. Faridi, *Prog. Org. Coat.,* 70 (2011) 39.

35. K.C. Chang, W.F. Ji, M.C. Lai, Y.R. Hsiao, C.H. Hsu, T.L. Chuang, Y. Wei, J.M. Yeh and W.R. Liu, *Polym. Chem.,* 5 (2014) 1049.
36. J.L. Trinstancho-Reyes, M. Sanchez-Carrillo, R. Sandoval-Jabalera, V.M. Orozco-Carmona, F. Almeraya-Calderón, J.G. Chacón-Nava, J.G. Gonzalez-Rodriguez and A. Martínez-Villafañe, *Int. J. Electrochem. Sci.,* 6 (2011) 419.